Electronic Supplementary Material (ESI) for Lab on a Chip.

Supporting Information

Rapid and label-free identification of single leukemia cells from blood in a high-density microfluidic trapping array by Fluorescence Lifetime Imaging Microscopy

Do-Hyun Lee,[†a] Xuan Li,[†a] Ning Ma,[*ab] Michelle A. Digman[*ab] and Abraham P. Lee[*a]

[a]*Department of Biomedical Engineering, University of California at Irvine, Irvine, CA, 92697, USA*

[b]*Laboratory for Fluorescence Dynamics, UC Irvine, CA, USA.*

* Corresponding authors:

Email: aplee@uci.edu (A.P. Lee.); Tel: +1 949-824-9691

Email: mdigman@uci.edu (M.A. Digman); Tel: 949-824-3255

† These authors contributed equally to this work.

Part I. Microfluidic isolation of single white blood cells in microwell arrays

To validate the separation and trapping principle we first tested the sorting and capturing capability of the device under various operational conditions (i.e., hematocrit and input flow rate) for an input stream of blood cell sample – WBC as a target cell for entrapment, RBC as a non-target cell (Fig. S2). The device was incubated with 1% (w/v) Pluronic F68 in PBS at room temperature prior to cell loading without blood cell attachment. The filtering capability of the pre-filter was examined. Cells were loaded into the microchannel using a syringe pump at the withdrawal mode under the flow rate of 0.2 mL/h for 5 min. The cell aggregates are expected to have a size of larger than 20 μm. Most of the single cancer cells and blood cells passed through the pre-filter, otherwise the cancer cell aggregates were still trapped at the pre-filter due to small pitch (25 μm width) and channel height (18 μm height). These cancer cells aggregates would cause the microchannel clogging at the trapping zone and decrease the single-cell occupancy. Under the flow rate of 0.2 mL/h, only 4.74% of cancer cell aggregates were flown through the pre-filter.

The comparison of percentage of microwell arrays that contain a single WBC ("single-cell occupancy") and >1 cell ("multi-cell occupancy") can be used to measure the performance of the trapping procedure. Also, we quantified the percentage of microwell arrays that contain a deformed single WBC due to the high shear stress. These deformed cells are located at the gap area instead of the trap, resulting in cell damage and preventing the observation of FLIM signal from the single cells. To investigate the effect of hematocrit on WBC capture in the microwell arrays, we first examined with diluted whole blood samples (0.5% to 10% hematocrit) (Fig. S1a–d) at a flow rate of 0.2 mL/h (Fig. S1e–h). The results explained that the multi-cell occupancy increased and with increasing hematocrit levels, while single-cell occupancy increased at lower concentration of hematocrit. With increased blood concentration, more RBCs tend to occupy the space between the traps and the loaded WBC instead of squeezing out, resulting in increase in multi-cell occupancy

and a decrease in the sorting efficiency at higher flow rates. In contrast, decreasing hematocrit facilitates rejecting RBCs and capturing single WBCs, thereby improving the sorting efficiency and the single-cell occupancy. However, a further decrease in the hematocrit to 0.5% required longer trapping time and induced prolonged shear stress to the already-trapped cells. Thus we chose to use 2% hematocrit for implementing both the throughput and the single-cell isolation performance.

Increasing flow rate reduces the cell trapping time to increase the throughput. We tested the trapping capability of the device in terms of the percentage of trapped single and multiple WBCs under various input flow rate from 0.2 to 1.0 mL/h. If the flow rate is increased to 1.0 mL/h for achieving higher throughput, the percentage of microwells that have multiple cells was decreased, however, the percentage of deformed single WBCs was dramatically increased up to 50.62%. This means that the high flow rate causes undesirable shear stress-induced cell deformation. The deformed cell would have low viability causing the FLIM signal readout to be inaccurate. Under an input flow rate of 0.2 mL/h, the percentage of intact single WBCs was about 56.09%, higher than other flow conditions. This results in a trade-off between the trapping efficiency and throughput. In addition, at higher flow rates, the pushing forces imposed on trapped single cells accelerate deformation and the trapped single cells can be released into the fluid stream from the single-cell trap without capturing. The higher number of released WBCs under the high pressure also affected the WBC recovery rate.

Part 2. Mathematic Explanation of the Phasor-FLIM Approach

The fluorescence lifetime data are acquired in the time domain for every pixel *(i, j)* of the image, and Fourier-transformed by the two following equations:

$$g_{i,g}(\omega) = \frac{\int_0^\infty I_{i,j}(t)cos(\omega t)dt}{\int_0^\infty I_{i,j}(t)dt} \quad \text{(S1)}$$

$$s_{i,g}(\omega) = \frac{\int_0^\infty I_{i,j}(t)sin(\omega t)dt}{\int_0^\infty I_{i,j}(t)dt} \quad \text{(S2)}$$

where $g_{i,g}(\omega)$ and $s_{i,g}(\omega)$ are the X and Y coordinates of the pixel's fluorescence lifetime decay da ta in the phasor plot; and $\omega = 2\pi f$ where f is the laser frequency (i.e., 80 MHz in our experiment). Therefore, every possible lifetime can be mapped into a specific point in the semicircle of the ph asor plot.

For a single exponential fluorescence lifetime decay $I(t)=Ae^{-t/\tau}$, which is the case for many p ure chemicals, e.g., pure NADH, its phasor coordinates are

$$g(\omega) = \frac{1}{1 + (\omega\tau)^2} \quad \text{(S3)}$$

$$s(\omega) = \frac{\omega\tau}{1 + (\omega\tau)^2} \quad \text{(S4)}$$

where τ is the decay lifetime and ω is the laser frequency. All single exponential lifetimes lie on t he "universal circle," defined as the semicircle going from (0, 0) to (1, 0), with radius of 1/2. Poi nt (0, 0) corresponds to $\tau = \infty$, and point (1, 0) corresponds to $\tau = 0$. Single-lifetime components c an be added directly in the phasor coordinates as the phasor follows the vector algebra. Therefore, a mixture of two distinct single-lifetime components, each of which lies separately on the semicir cle, lies along the line joining the two lifetime points (inside the semicircle).

As for a system with multiple fluorescent components, like a cell, the overall decay is a pha sor that is the sum of the independent phasors of each fluorescence component:

$$G(\omega) = \sum_{1}^{n} f_n g_n(\omega) \tag{S5}$$

$$S(\omega) = \sum_{1}^{n} f_n s_n(\omega) \tag{S6}$$

where f_n is the fractional contribution of each component (g_n, s_n). A mixture of two multi-exponential decay species, i.e., two specific phasor points inside the semicircle, lies along the line joining the two points. Similarly, a mixture of three species locates inside a triangle connecting the three points, and etc.

Part 3. Mathematic Explanation of the Multi-parametric Separation Scheme

While WBCs were distinguished from leukemia cells by the average *(g,s)* values of each single cells' phasor plot, different types of leukemia cells were not fully separated through this simple approach, and there lacked of a quantitative description. To achieve a more precise and quantitative separation, the 2D phasor plot of each cell was viewed as a 3D phasor distribution by adding the counts of phasor points at each *(g,s)* location as the *z* axis. As illustrated in Fig. S3 (a) and (b),[25] the phasor histogram was split in four equidistance segments based on the height of the peak, and the average *(g,s)* values were calculated in each segment, generating a spectrum of 8 parameters.

When separating two cell populations, T (test) and C (control), a training set was established, where each cell *k* has a spectrum *f(i,k)* consisted of 8 parameters. For every cell in the T group, its deviation from the average spectrum of the two groups was calculated by:

$$DF_T(k) = \sum_{i} \left(T_{av}(i) - f(i,k)\right)^2 w(i)/8 \tag{S7}$$

$$DF_C(k) = \sum_{i} \left(C_{av}(i) - f(i,k)\right)^2 w(i)/8 \tag{S8}$$

The same calculation was performed for each cell in the C group to get DC_T and DC_C. The weigh

ts *w(i)* for each parameter varied from 0 to 1 and were normalized so that the sum was a constant. The *w(i)* were used to emphasize which parameter was more important to achieve a better separatio n, and a quantity, Distance (D), was built to determine *w(i)* by minimization algorithm:

$$D = \min\left[\sum_k \left(DF_T(k) + \frac{1}{DF_C(k)} + DC_C(k) + \frac{1}{DC_T(k)}\right)\right] \quad \text{(S9)}$$

If *w(i)* = 0, the corresponding parameter did not influence D. If *w(i)* = 1, it had a maximum influe nce. This algorithm found parameter combinations to minimize the distance between the cells of one group from the group average and maximize the distance from the other group's average. Aft er minimization, we got the values of the weights that best separated the two cell populations of t he training set. An unknown sample was loaded to the training set, and its position was obtained using the separation index SI defined as

$$SI(k) = 10 \times \frac{\left(DX_C(k) - DX_T(k)\right)}{\left(DX_C(k) + DX_T(k)\right)} \quad \text{(S10)}$$

where X was the measurement of the unknown. In explain, if X was equal of the average of C gr oup, then SI = -10; while if it was equal to the average of T group, then SI = +10. An SI histogra m was plotted to determine if a cell was a true positive (below 0, same as the C group) or false p ositive (above 0, fell into the T group). Statistical methods such as the area-under-the-curve (AU C) values were used to determine the quality of the training set.

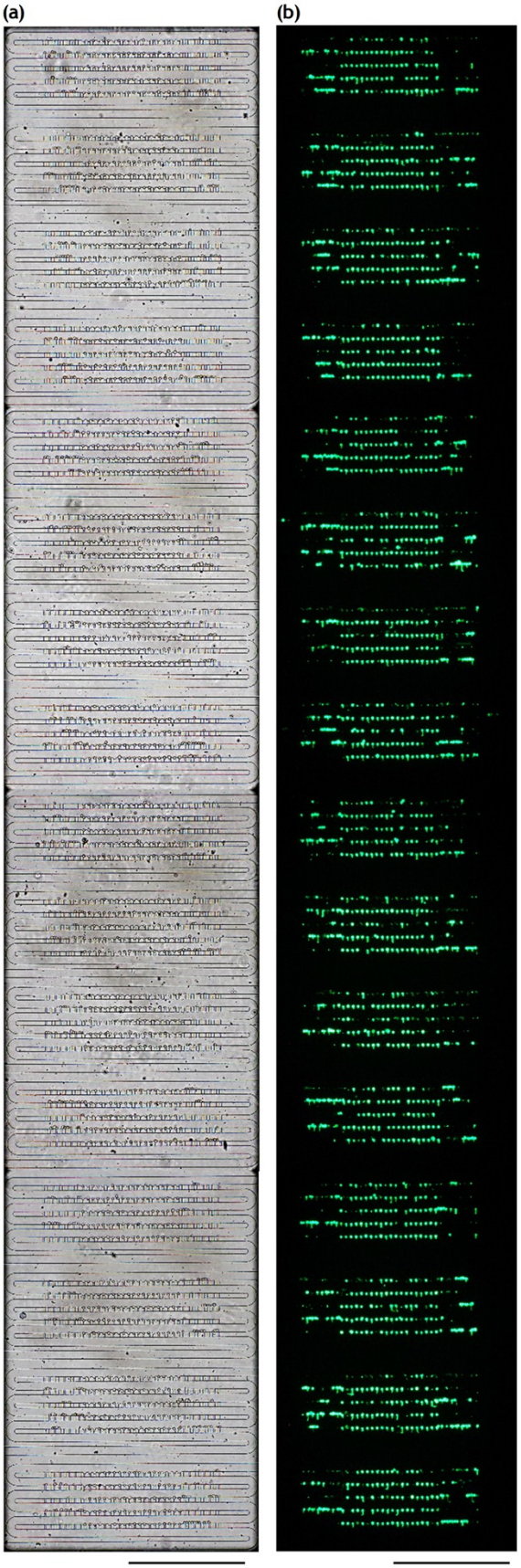
(a)
(b)

Figure S1. 1600 single cell traps filled with K562 cells. The bright-field (a) and fluorescent (b) images of the presented high-throughput microfluidic trapping array consisted of 16 identical arrays of highly packed 100 single-cell traps. Scale bar: 1 mm.

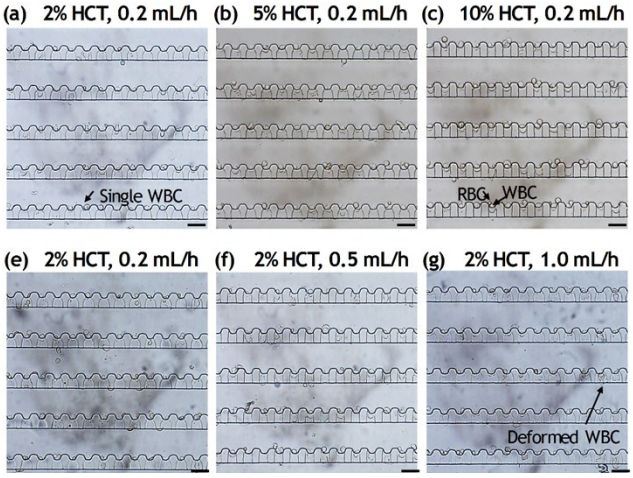

Figure S2. Characterizing trapping efficiency of the microfluidic device with various operational conditions. Representative bright-field microscopic images illustrating the effect of (a–c) hematocrit and (e–g) flow rate on single WBC trapping. (a) 2%; (b) 5%; (c) 10% hematocrit with 0.2 mL/h input flow rate. (d) Plot showing trap single-cell and multiple-cell occupancy for varying hematocrits. (e) 0.2 mL/h; (f) 0.5 mL/h; (g) 1.0 mL/h hematocrit with 2% hematocrit. (h) Plot showing the percentage of trapped intact single, deformed single WBCs and multiple WBCs. Scale bars: 50 μm.

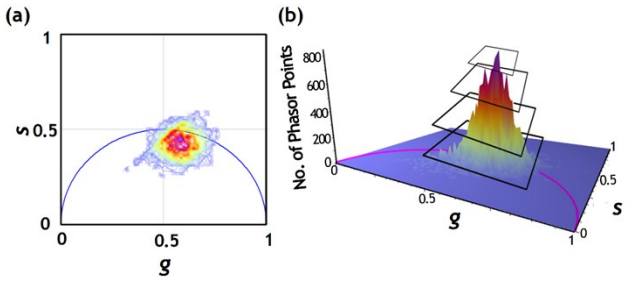

Figure S3. Transforming a 2D phasor plot into a 3D phasor distribution plot.[25] The phasor points in the 2D phasor heat map (a) was plotted in a 3D format (b) where the count of phasor points at each *(g,s)* location is added as the z axis. The 3D phasor distribution was split in four equal height segments, and the average *g* and *s* values at each segments were calculated to collect a total of 8 parameters.

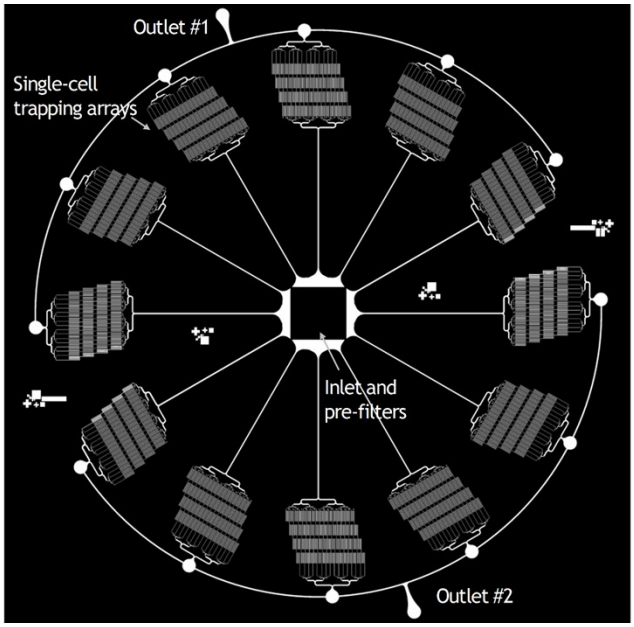

Figure S4. Schematic illustration of a paralleled device with 12 individual channels radially arrayed with a single inlet and two ring outlets. It is anticipated that when 2% diluted blood is tested at 0.2 mL/h, 72,000 single cancer cells and WBCs can be isolated in 6 min.

Supporting Movie Captions

Supplemental Movie S1. Isolation of single WBCs from diluted blood sample. A video demonstrating isolation of single cancer cells and WBCs. Test was operated at a flow rate of 0.2 mL/h.

Supplemental Movie S2. Continuous RBC filtration via the gap area. A video demonstrating removal of RBCs via the gap area taken using a high-speed camera. The gap area makes the perpendicular flow to deform and migrate RBCs, while WBCs and leukemia cells can be pushed into traps, and the combination of perpendicular deformation and horizontal delivery flow enables the continuous blood cell filtration process.